nature structural & molecular biology

BRIEF COMMUNICATION

https://doi.org/10.1038/s41594-019-0254-6

Crystal structure of the tubulin tyrosine carboxypeptidase complex VASH1–SVBP

Athanassios Adamopoulos[1,2,7], Lisa Landskron[1,2,7], Tatjana Heidebrecht[1,2], Foteini Tsakou[1], Onno B. Bleijerveld[3], Maarten Altelaar[3,4], Joppe Nieuwenhuis[1,2], Patrick H. N. Celie[1], Thijn R. Brummelkamp[1,2,5,6] and Anastassis Perrakis[1,2*]

The cyclic enzymatic removal and ligation of the C-terminal tyrosine of α-tubulin generates heterogeneous microtubules and affects their functions. Here we describe the crystal and solution structure of the tubulin carboxypeptidase complex between vasohibin (VASH1) and small vasohibin-binding protein (SVBP), which folds in a long helix, which stabilizes the VASH1 catalytic domain. This structure, combined with molecular docking and mutagenesis experiments, reveals which residues are responsible for recognition and cleavage of the tubulin C-terminal tyrosine.

Microtubules are key components of the eukaryotic cytoskeleton, involved in cell division, morphogenesis, motility and intracellular transport. Post-translational modifications of tubulin heterodimers, the so-called 'tubulin code', includes the enzymatic removal and ligation of the C-terminal tyrosine[1]. Although the tubulin tyrosine ligase that reverts α-tubulin to the translated form has been described[2] and structurally characterized[3,4], the carboxypeptidase that removes it has remained elusive for four decades. Recently, we[5] and others[6] described a complex between SVBP, a 66-residue peptide, and vasohibins (VASH1 or VASH2), as the long-sought-for tubulin carboxypeptidases. Vasohibins increase detyrosination of α-tubulin in cells and in vitro[5], especially in the presence of SVBP, and both proteins have been implicated in neuronal function, a role that may be associated with their role in tubulin detyrosination[6].

A chaperone-like function was possible because SVBP enhances the levels of detyrosinated α-tubulin, and concomitantly affects the cellular abundance and solubility of vasohibins. VASH1 might have a transglutaminase-like protease fold, with a non-canonical Cys-His-Ser catalytic triad[7]; however, low similarity to existing structures precludes establishment of a reliable structural model. To study the folding of VASH1, to understand how SVBP affects vasohibins and to examine how VASH1 recognizes and cleaves the α-tubulin C-terminal tyrosine, we co-expressed a VASH1–SVBP complex in insect cells, and then purified and crystallized it. The crystal structure was determined by sulfur single-wavelength anomalous dispersion (S-SAD) phasing, notably averaging 16 data sets of 360° sweeps using a PRIGo multi-axis goniometer[8]. The structure was refined to 2.1 Å resolution to an R_{free} of 21.4% (see Methods and Supplementary Table 1 for crystallographic details).

Only residues 60–304 of VASH1 (1–315 expressed) and 26–52 of SVBP (1–66) were visible in the electron density maps and modeled (Fig. 1a). The VASH1–SVBP complex has a compact structure (Fig. 1b,c): SVBP forms a slightly bent α-helix that inserts between a short N-terminal two-helix bundle domain of VASH1 (60–97) connected to an α/β fold C-terminal domain (118–304) comprised of five α-helices and a five-stranded antiparallel β-sheet flanked by helices, adopting a classic papain-like cysteine protease fold. An impressive 40% (1,164 Å)^2 of the total surface area of SVBP is buried upon complex formation with VASH1. The interface between SVBP and VASH1 contains 14 hydrogen bonds between the side chains of seven SVBP residues (Arg34, Gln35, Arg36, Glu38, Tyr40, Asn43, Thr47) and VASH1, and two salt bridges, both formed between Lys32 of SVBP and Glu163 of VASH1 (Fig. 1d). Notably, only two side chains of VASH1 (Gln133 and His136) interact with SVBP; all other VASH1 hydrogen bonds involve main chain atoms. The SVBP helix residues that interact with SVBP are well-conserved (Supplementary Figs. 1 and 2a), in contrast to the less well-conserved VASH1 interaction interface that predominantly involves main chain atoms. Mutations of key residues in SVBP (and most notably Lys32, Gln35, Arg36, Asn43, which make two or three hydrogen bonds to VASH1) reduced VASH1 expression and decreased detyrosination in HeLa cells co-transfected with both proteins (Fig. 1e, Methods and Supplementary Fig. 2b). This confirms a role for SVBP as a structural chaperone and highlights the importance of specific interactions between VASH1 and SVBP.

The fit of the VASH1–SVBP crystal structure to small angle X-ray scattering (SAXS) data obtained for the full-length complex[5] is poor (Fig. 2a), and the dimensionless Kratky plot (Fig. 2a inset) suggests a folded but elongated particle[9] for the full-length VASH1–SVBP monomer (Supplementary Fig. 3a). The poorly conserved N terminus and the well-conserved C terminus of VASH1 (Supplementary Fig. 1), as well as both termini of SVBP, were disordered in our structure. Using the BUNCH program[10] to model the disordered termini in the SAXS data yielded extended conformations suggestive of unstructured regions (Fig. 2a, inset). This model, however, does not fully explain the Kratky plot, implying they exist in multiple conformations[9], behaving as intrinsically disordered regions (IDRs). We speculate that the conserved IDR C terminus of VASH1 could interact with tubulin or other cellular factors.

The active site nucleophile of VASH1, Cys169, resides within the VASH1 catalytic papain-like domain. It is positioned in the middle of a groove of well-conserved residues (Fig. 2b), predominantly arginine and lysine, which give rise to a positive electrostatic

[1]Division of Biochemistry, the Netherlands Cancer Institute, Amsterdam, the Netherlands. [2]Oncode Institute, Division of Biochemistry, the Netherlands Cancer Institute, Amsterdam, the Netherlands. [3]Proteomics Facility, the Netherlands Cancer Institute, Amsterdam, the Netherlands. [4]Biomolecular Mass Spectrometry and Proteomics, Bijvoet Center for Biomolecular Research and Utrecht Institute for Pharmaceutical Sciences, Utrecht University, Utrecht, the Netherlands. [5]CeMM Research Center for Molecular Medicine of the Austrian Academy of Sciences, Vienna, Austria. [6]Cancer Genomics Center, Amsterdam, the Netherlands. [7]These authors contributed equally: Athanassios Adamopoulos, Lisa Landskron. *e-mail: a.perrakis@nki.nl

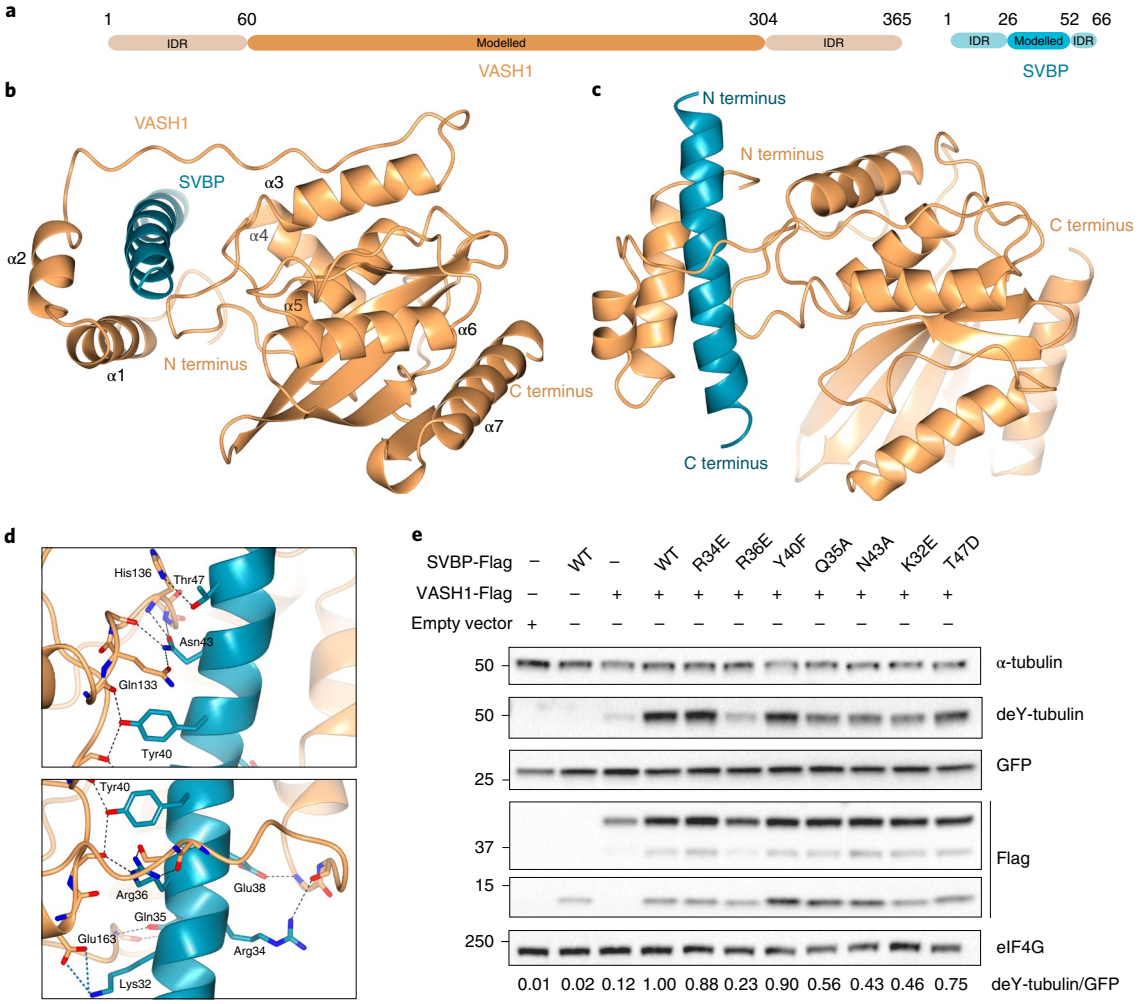

Fig. 1 | X-ray structure of the human VASH1–SVBP complex. **a**, Domain organization of VASH1 and SVBP. **b**,**c**, Ribbon representation of the structure. **d**, Interacting residues in the complex interface shown as cylinders; the interaction network is shown as dotted lines (black, hydrogen bonds; blue, salt bridges). **e**, Western blots showing the expression and detyrosination effects of SVBP mutants in the VASH1 interface; quantification of detyrosination activity is based on two replicates (Supplementary Fig. 3); uncropped blot images are shown in Supplementary Data Set 1. WT, wild type.

potential (Fig. 2c). This groove is thus ideally suited for binding the electronegative glutamate-rich C-terminal tail of tubulin (…EGEGEEEGEEY). Semi-quantitative mass spectrometry (MS) analysis of VASH1–SVBP-mediated cleavage of 12-mer tubulin tail peptide mutants (where glutamates are converted to alanine and glycines to proline) showed that the only mutation that affected substrate cleavage, other than the mutation to alanine or deletion of the terminal tyrosine, was that of the second last glutamate (E-2). All other mutations processed with efficiency similar to the wild-type terminal peptide (Supplementary Fig. 3b and Methods).

With that information at hand, we used the high ambiguity driven biomolecular docking approach in HADDOCK[11] to suggest a binding mode for a short C-terminal peptide of tubulin (EGEEY) to VASH1. We obtained several clusters of computational models (for details, see Methods and Supplementary Table 2). Using a representative model of the most populous cluster (Supplementary Fig. 3c), we designed a series of VASH1 mutants. The activity of these mutants was examined by monitoring the level of detyrosination in cells, identifying Lys146, Lys168 and Arg222 as critical residues. Using this additional information and a longer peptide (GEEEGEEY), we performed a second round of modeling in HADDOCK, which suggested a unique cluster of models for peptide binding (Fig. 2d; for details, see Methods and Supplementary Table 3).

The predictions from this model were quantitatively validated in cells (Fig. 3 and Supplementary Fig. 4). The suggested catalytic triad[7], which includes the nucleophile Cys169 that is activated by His204, is supported by our model (Fig. 3a); as expected, both the C169A and H204A mutations entirely abolished catalytic activity (Fig. 3b). The text-book mechanism[12], and a structural search for folds similar to the VASH1 catalytic domain (see Supplementary Fig. 5, Supplementary Table 4 and Methods for details) showed that a negatively charged residue (aspartate or glutamate) stabilizes the protonated state of the histidine. Although such a negatively charged residue is not obvious in VASH1, this might be provided by the main chain carbonyl of Leu226. The nucleophilic attack by Cys169 results in release of the terminal tyrosine, leaving an anionic transient thioester intermediate. Ser221 could act as a hydrogen donor to fulfill this role, similar to Asn93 of the structurally related *Pseudomonas avirulence* AvrPphB protease[13] (Supplementary Fig. 5e). Indeed, Ser221A has only 7% of the wild-type activity, consistent with a role in catalysis.

VASH1–SVBP acts as a carboxypeptidase specific for the C-terminal tyrosine. The terminal carboxyl group is predicted to contact Arg222 and Tyr134 in our model (Fig. 3c). Indeed, the R222E and Y134F mutants retain only 1% and 23% of the activity (Fig. 3d). According to our model, Lys168 could also be involved

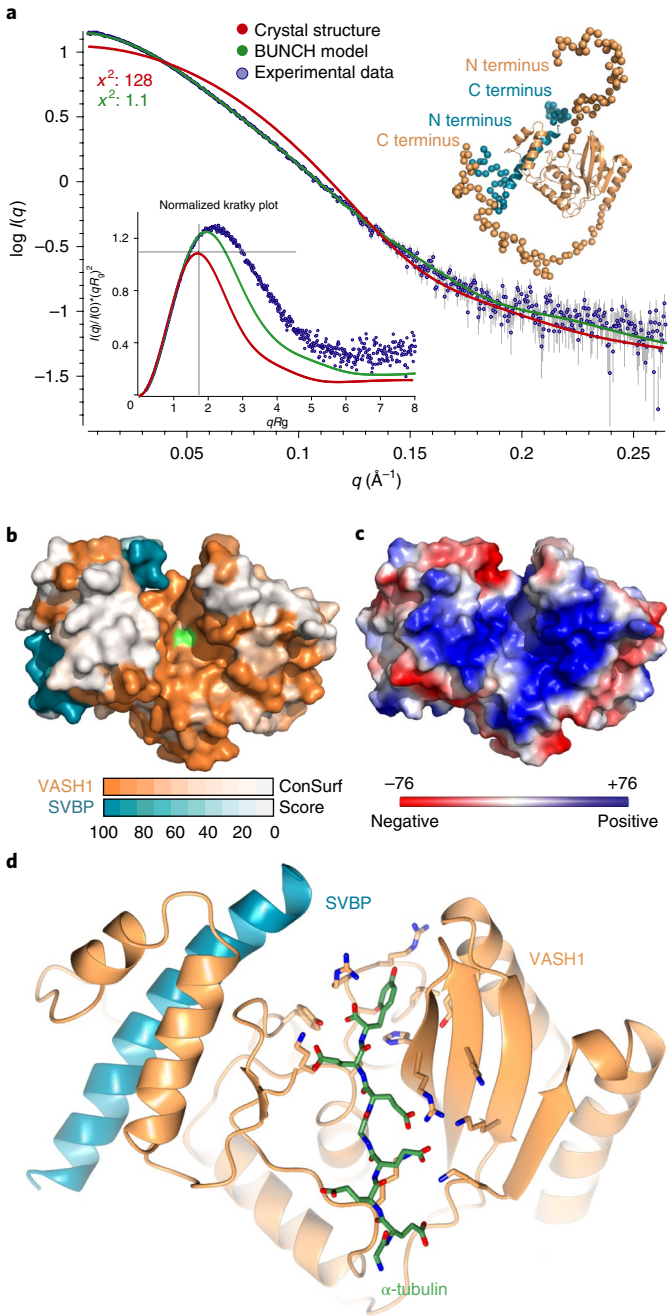

Fig. 2 | Structural analysis of the VASH1–SVBP complex. a, Comparison of the SAXS data (blue), theoretical curve from the crystal structure (red) and the BUNCH model (green). The corresponding dimensionless Kratky plot is shown as an inset (the cross-hair corresponds to the peak position for a well-ordered approximately spherical structure); the BUNCH model with the missing N and C termini shown as spheres is also as an inset. R_g, radius of gyration; q, scattering vector; θ, half the scattering angle; λ, wavelength of the incident beam; $I(q)$, scattering intensity; $I(0)$, forward scattering intensity. **b**, Surface representation of the VASH1–SVBP complex colored by sequence conservation; the active site Cys169 is shown in light green. **c**, Surface representation of the VASH1–SVBP complex colored by electrostatic potential (k_BT/e). **d**, Ribbon representation of a representative computational model of the complex between VASH1–SVBP and the tubulin tail peptide (GEEEGEEY); the peptide and residues involved in binding and catalysis are shown as cylinders.

in recognition of the carboxyl group, or of the E-1 glutamate of the tubulin tail. The K168E mutant retains only 10% of the activity and, based on our MS results, we hypothesize that Lys168 is more important for the carboxyl recognition. The terminal tyrosine side chain does not show any obvious interactions in our model, except for a weak hydrophobic packing with Leu226; the L226A reduces activity to 45% of the wild type. We note, however, that the L226A substitution might also affect positioning of the Leu226 main chain carbonyl and thus the stabilization of the protonated state of His204. As expected from our model, the R223A and Y247F mutants do not significantly affect activity.

The MS analysis indicated that the second last glutamate (E-2) is crucial for substrate recognition. Based on our model, E-2 is recognized by Lys146 (Fig. 3e); indeed, the K146E mutant retains only 19% of the wild-type activity (Fig. 3f). Mutation of the nearby well-conserved Arg203 and Lys258 (R203E, K258E) affected activity by only about 20%; the double mutant, however, lost 70% of the activity compared to wild type, suggesting that the network of positive (VASH1) and negative (tubulin) residues is important, but has some degree of redundancy. Mutation of the Lys276 (contacting the E-4 glutamate) to glutamate had no significant effect in activity, consistently with MS analysis.

Our crystal structure established that SVBP stabilizes a helical N-terminal domain of VASH1 in a catalytic papain-like cysteine protease fold. SAXS data imply the existence of well-conserved IDRs at the termini of both proteins. The computational model for binding to the tubulin tail was validated by mutagenesis experiments and activity assays in cells, offering a window into catalysis and substrate recognition. This work provides a scaffold for inhibitor or probe design for further study of the biology of tyrosine carboxypeptidases.

Online content

Any methods, additional references, Nature Research reporting summaries, source data, statements of code and data availability and associated accession codes are available at https://doi.org/10.1038/s41594-019-0254-6.

Received: 6 February 2019; Accepted: 16 May 2019;
Published online: 1 July 2019

References

1. Wehenkel, A. & Janke, C. *Nat. Cell Biol.* **16**, 303–305 (2014).
2. Murofushi, H. *J. Biochem.* **87**, 979–984 (1980).
3. Prota, A. E. et al. *J. Cell Biol.* **200**, 259–270 (2013).
4. Szyk, A., Deaconescu, A. M., Piszczek, G. & Roll-Mecak, A. *Nat. Struct. Mol. Biol.* **18**, 1250–1258 (2011).
5. Nieuwenhuis, J. et al. *Science* **358**, eaao5676–1456 (2017).
6. Aillaud, C. et al. *Science* **358**, 1448–1453 (2017).
7. Sanchez-Pulido, L. & Ponting, C. P. *Bioinformatics* **32**, 1441–1445 (2016).
8. Waltersperger, S. et al. *J. Synchrotron Radiat.* **22**, 895–900 (2015).
9. Rambo, R. P. & Tainer, J. A. *Biopolymers* **95**, 559–571 (2011).
10. Petoukhov, M. V. & Svergun, D. I. *Biophys J* **89**, 1237–1250 (2005).
11. van Zundert, G. C. P. et al. *J. Mol. Biol.* **428**, 720–725 (2016).
12. Otto, H.-H. & Schirmeister, T. *Chem. Rev.* **97**, 133–172 (1997).
13. Zhu, M., Shao, F., Innes, R. W., Dixon, J. E. & Xu, Z. *Proc. Natl Acad. Sci. USA* **101**, 302–307 (2004).

Acknowledgements

We thank V. Olieric for help with S-SAD phasing and data collection at PXIII at the SLS Synchrotron, and the MASSIF beamline team at the ESRF for native data collection. The authors received the following funding support: grant no. NWO 184.032.201 to M.A.; grant nos. NWO 016.Vici.170.033 and KWF NKI-2015–7609, support by the Cancer Genomics Center (CGC.nl) and an Ammodo KNAW Award 2015 to T.R.B.; support by the Oncode Institute to T.R.B. and A.P.

Author contributions

A.A. performed and analyzed biochemical and structural experiments, wrote a draft manuscript and prepared figures. L.L. performed and analyzed cell-based experiments and prepared figures. T.H. participated in protein purification, crystallization and data collection. F.T. performed expression tests and produced initial crystals, under supervision of A.A. and P.C. O.B.B. and M.A. analyzed the MS samples prepared by J.N. A.P. participated in crystallographic data analysis, wrote the final manuscript and supervised the project together with T.R.B.

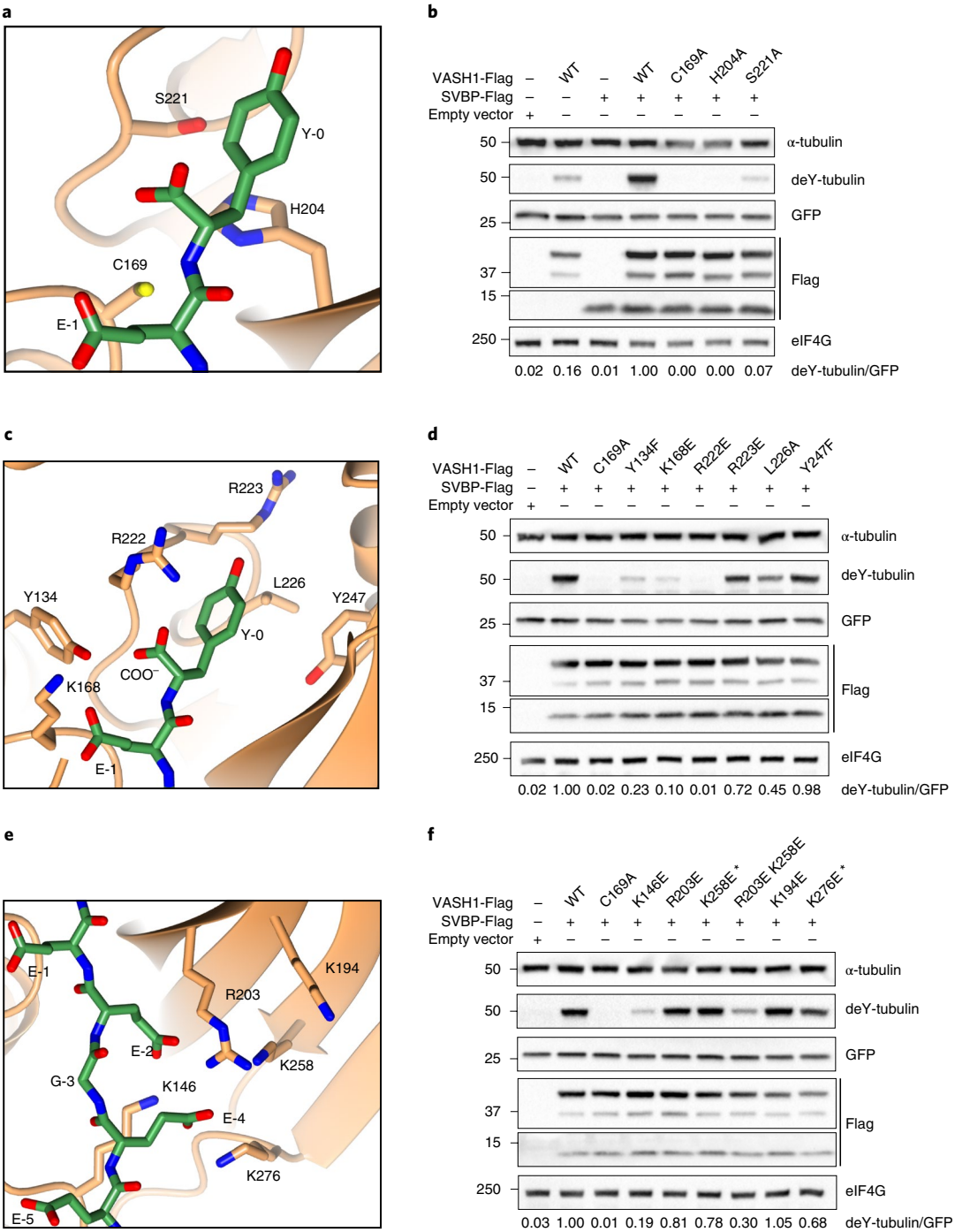

Fig. 3 | Tubulin tail binding and recognition. a–e, Close-up focusing on mutated residues (**a**, **c** and **e**) whose activity in cells is shown, respectively, in **b** (active site residues), **d** (terminal tyrosine recognition) and **f** (glutamates recognition). Quantification of detyrosination activity is based on two replicates (Supplementary Fig. 7a–c); the asterisk denotes mutants that contained an additional mutation (H80Y) that has no effect on activity compared to the wild type (Supplementary Fig. 7d,e); uncropped blot images are shown in Supplementary Data Set 1.

Competing interests

T.R.B. is co-founder and SAB member of Haplogen GmbH and co-founder and managing director of Scenic Biotech. All other authors declare no competing interests.

Additional information

Supplementary information is available for this article at https://doi.org/10.1038/s41594-019-0254-6.

Reprints and permissions information is available at www.nature.com/reprints.

Correspondence and requests for materials should be addressed to A.P.

Peer review information: Beth Moorefield was the primary editor on this article and managed its editorial process and peer review in collaboration with the rest of the editorial team.

Publisher's note: Springer Nature remains neutral with regard to jurisdictional claims in published maps and institutional affiliations.

Methods

Cloning expression and purification. A truncation construct of VASH1 (1–315) inactive mutant (C169A) and the full-length SVBP peptide were expressed in *Spodoptera frugiperda* (Sf9) insect cells using the Invitrogen Bac-to-Bac method as described previously[5]. Briefly, VASH1 was cloned in a modified pFastBac1 with a 3C cleavable C-terminal double-strep and 10His tag[14]. The complex was expressed in Sf9 insect cells using Insect-Xpress media (LONZA). Cells were grown in a shaker at 28 °C and infected at a density of 2×10^6 cells ml^{-1}. Cells were harvested 72 h post-infection, and the biomass was flash frozen in liquid nitrogen and stored at −20 °C. The purification protocol described previously[1] was used with the following modifications. A two-step affinity purification scheme was employed, using first a Ni-NTA (Qiagen) affinity purification step, followed by Streptactin superflow resin (IBA) affinity purification. The tags were removed using 3C-protease overnight at 4 °C. The VASH1–SVBP complex was further purified by size-exclusion chromatography on a Superdex S-200 column (GE Healthcare) in 20 mM HEPES/NaOH pH 7.5, 100 mM NaCl and 1 mM Tris(2-carboxyethyl) phosphine. The purified protein was concentrated with a 3 kDa centrifugal concentrator (Amicon) to a final concentration of 3.5 mg ml^{-1}, flash frozen and stored at −80 °C until further use.

Crystallization. Initial screening was performed using the commercial screens PACT, JCSG+, Classics-I & II, ProComplex, ComPAS, pH-Clear and Morpheus. Hits were identified in the PACT screen[15] and further optimized by using Linbro plates. VASH1–SVBP diffracting crystals were obtained in 0.1 M Tris pH 8.8, 0.2 M $CaCl_2$ and 19% PEG 3000. Crystals grew to maximum dimensions over a period of 2 weeks. Crystals were harvested and cryo-protected in a solution containing 30% glycerol and vitrified in liquid nitrogen. A native data set was collected at beamline ID30A (MASSIF)[16] at the ESRF to 2.1 Å resolution. Diffraction data were integrated and scaled automatically by XDS[17] (Supplementary Table 1).

Structure solution and refinement. A native crystal was chosen for structure determination based on the intrinsic sulfur anomalous signal. Using the PRIGo[8] goniometer, we collected 16 different data sets at a wavelength of 2.075 Å at the PSI X06DA beamline (PXIII) (Villingen, Switzerland). Each data set was a full 360° sweep with an oscillation angle of 0.2° and a total exposure time of 180 s (with an estimated total dose of 0.5 MGy). The first ten data sets were collected stepping the χ angle by 5° between data sets, and the six subsequent data sets were collected stepping the ϕ angle by 10° between data sets. In each individual data set, the R_{merge} of the lowest resolution shell was between 7% and 12% and the signal-to-noise ratio of the anomalous signal was only slightly above unity. These discouraging statistics were most likely caused by smaller satellite crystals that were present, giving rise to multiple lattices in the diffraction pattern at low resolution. Averaging all 16 data sets gave rise to a single data set with an average multiplicity of 72 times, giving rise to a low resolution shell signal-to-noise ratio of the anomalous signal close to three, extending to about 2.8 Å resolution. The anomalous correlation coefficient was above 0.9 at the lowest resolution shell and 0.3 at about 2.8 Å resolution.

The HKL2MAP interface[18] was used to run the SHELX[19] programs suite, using different resolution cutoffs and different number of sites. Eight sites at 2.8 Å resolution gave the most convincing solutions, with a few SHELXD trials having a higher correlation coefficient for both all and the weak reflections. The best solution identified nine sulfur sites with occupancy between 0.8 and 1.0, with the tenth site having an occupancy of 0.53. We considered this a likely solution, and we ran the CRANK pipeline[20] using these sites as input. CRANK resulted in a model containing 280 residues in six fragments; 86% of the residues were docked in sequence. Using this model, we obtained a molecular replacement solution against the native data set.

The structure was completed manually and refined by several iterations of REFMAC5[21] and manual rebuilding in COOT[22], including a few runs of the PDB-REDO pipeline[23]. The final model has an R_{free} of 0.214, is in the 100th percentile of Molprobity (0.82) and has a clash score (0.89)[24] with no Ramachandran outliers (Supplementary Table 1).

Small angle X-ray scattering. Data for the VASH1–SVBP complex were recorded and analysed as described previously. BUNCH[10] from the ATSAS suite[25] was used to add the missing residues to the crystal structure of VASH1–SVBP using the default settings. Theoretical scattering data from VASH1 and SVBP atomic models were generated using CRYSOL[26].

VASH1 substrate specificity analysis by liquid chromatography–tandem mass spectrometry. Peptides incubated with active VASH1 were analyzed on a Thermo Orbitrap Fusion hybrid mass spectrometer (Q-OT-qIT, Thermo Fisher Scientific, Bremen) equipped with a Proxeon nLC 1000 system (Thermo Fisher Scientific) fitted with a 75 µm × 500 mm analytical column (ReproSil-Pur 120 C18-AQ 2.4 µm (Dr. Maisch GmbH) packed in-house). Solvent A was 0.1% formic acid and peptides were eluted from the column in a 45-min gradient containing a 30-min linear increase from 10–40% solvent B (80% acetontrile/0.1% formic acid). Survey scans of peptide precursors from m/z 375–1,500 were performed at 120 K resolution in the Orbitrap with a 4×10^5 ion count target. Tandem MS was performed by higher-energy collisional dissociation fragmentation with normalized collision energy of 20 eV and ion trap MS2 fragment detection. The MS2 ion count target was set to 10^4 and the maximum injection time was set to 50 ms. The instrument was run in top speed mode with 3 s cycles.

Raw data files were processed using Proteome Discoverer (v.1.4.0.288, Thermo Fisher Scientific). MS2 spectra were searched against a custom database containing the mutagenized synthetic versions of the tubulin-like C-terminal peptides, using Mascot (v.2.6.1, Matrix Science, UK). No miscleavages were allowed and data was filtered with ion score > 20. Determination of the extent of peptide cleavage by VASH1, and subsequent assessment of VASH1 substrate specificity, was performed based on the number of peptide spectrum matches for the intact and cleaved/detyrosinated version of each peptide.

Docking. A work-in-progress model of the VASH1–SVBP complex was used for a computational experiment using high ambiguity driven docking (HADDOCK[11,27]). First, we created an extended conformation of a minimal substrate peptide with the sequence EGEEY. For the docking we defined the terminal tyrosine and the second last glutamate as active residues for the substrate. For the VASH1–SVBP complex, we only defined that the γ-S of the catalytic Cys169 should be in contact with the carbonyl carbon of the scissile bond. All other parameters were used with default values. HADDOCK clustered 143 models into 9 clusters (Supplementary Table 2), of which the largest cluster contained 62 models. A representative of this cluster was used for designing validation experiments by site directed mutagenesis.

For the second modeling round, we first created an extended conformation of a minimal substrate peptide with the sequence GEEEGEEY. For the docking we defined the terminal tyrosine and the second last glutamate as active residues for the substrate. For the VASH1–SVBP complex we defined that the γ-S of the catalytic Cys169 should be in contact with the carbonyl carbon of the scissile bond and Lys146, Lys168 and Arg222 as active residues. All other parameters were used with default values. HADDOCK clustered all 198 models in one cluster. The HADDOCK score for this cluster was −165.2, significantly better than −108.3 in the previous modeling round (Supplementary Table 3).

Structure similarity searches. Structure similarity searches were carried out by DALI[28] searches, using a truncated version of the VASH1 catalytic core (residues 118–304) against the whole PDB. The top hits (Z-score > 6.0) were analyzed by manual inspection (Supplementary Table 4 and Supplementary Fig. 5).

Conservation analysis. A multiple sequence alignment with sequences for VASH1 from different model organisms was prepared using CLUSTAL-OMEGA[29] through the EBI service portal[30]. We then used the ConSurf webserver[31] to calculate the conservation scores, using default values and the Bayesian method. Visualization of the results was done with PyMOL.

Mutagenesis. VASH1 and SVBP site-specific mutants were created using the QuikChange strategy (Stratagene). All constructs were verified by sequencing.

Detyrosination assay. The peptide detyrosination assay to determine substrate specificity of the VASH1–SVBP complex was performed as previously described in Nieuwenhuis et al.[5]. 500 nM VASH1–SVBP complex was incubated with 500 µM of the indicated peptide in buffer containing 50 mM Tris-HCl pH 8.0, 10% glycerol, 1 mM DTT and 1 mM PMSF, and was incubated for 2 h at 37 °C. All peptides were dissolved in general tubulin buffer containing 80 mM PIPES pH 6.9, 2 mM $MgCl_2$ and 0.5 mM EGTA.

To measure detyrosination activity in cells, constructs of Flag-tagged VASH1 and SVBP were transfected into H1 HeLa cells using lipofectamine 2000. To control for transfection efficiency between samples, a green fluorescent protein (GFP)-expressing plasmid was co-transfected. Cells were washed with PBS and then harvested directly in sample buffer (0.25 M Tris-HCl pH 6.8; 6% SDS, 30% glycerol, 16% β-mercaptoethanol and bromophenolblue). Boiled samples were run on 4–12% Bis-Tris gels in MOPS buffer. Blotting was performed using standard blotting buffer with 20% ethanol. After blocking in 4% milk in 0.1% TBS-Tween (blocking solution), blots were incubated with antibodies in blocking solution. Antibodies used were to eIF4G (Cell Signaling Technologies, no. 2498); α-tubulin (DM1A; Santa Cruz Biotechnology, no. 32293), Flag (Cell Signaling Technologies, no. 2368), detyrosinated tubulin (Merck Millipore AB3201) and GFP (Santa Cruz Biotechnology, no. 8334). After membrane washing, blots were incubated with horseradish-peroxidase-coupled secondary antibodies, washed and developed using standard enhanced chemiluminescence reagents.

Detyrosination levels were quantified in the software Fiji. To measure the levels of GFP and detyrosinated tubulin, same-sized rectangles were used to measure the raw integrated density (sum of pixel values) of each sample. The background (defined as the measurement in the rectangle on an empty area of the blot) was subtracted from each measurement and the detyrosinated tubulin/GFP ratio was calculated. Ratios were normalized to the control (wild-type SVBP + VASH1).

Cell lines used. H1 HeLa were purchased from ATCC (catalog no. CRL-1958), tested for mycoplasma and were not authenticated.

Reporting Summary. Further information on research design is available in the Nature Research Reporting Summary linked to this article.

Data availability

The coordinates for the crystal structure of the VASH1–SVBP complex are deposited in the PDB under the accession identifier PDB 6NVQ. All other data and the coordinates of the HADDOCK model are available upon request.

References

14. Luna-Vargas, M. P. A. et al. *J. Struct. Biol.* **175**, 113–119 (2011).
15. Newman, J. et al. *Acta Crystallogr. D Biol. Crystallogr.* **61**, 1426–1431 (2005).
16. Nurizzo, D. et al. *Acta Crystallogr. D Struct. Biol.* **72**, 966–975 (2016).
17. Kabsch, W. *Acta Crystallogr. D Biol. Crystallogr.* **66**, 125–132 (2010).
18. Pape, T. & Schneider, T. *J. Synchr. Rad.* **37**, 843–844 (2004).
19. Uson, I. & Sheldrick, G. *Curr. Opin. Struct. Biol.* **9**, 643–648 (1999).
20. Ness, S., de Graaff, R., Abrahams, J. & Pannu, N. *Struct. Solut. Struct. (Camb.)* **12**, 1753–1761 (2004).
21. Murshudov, G. N. et al. *Macromol. Cryst. Struct.* **67**, 355–367 (2011).
22. Emsley, P., Lohkamp, B., Scott, W. G. & Cowtan, K. *Acta Crystallogr. D Biol. Crystallogr.* **66**, 486–501 (2010).
23. Joosten, R. P., Long, F., Murshudov, G. N. & Perrakis, A. *IUCrJ* **1**, 213–220 (2014).
24. Chen, V. B. et al. *Acta Crystallogr. D Biol. Crystallogr.* **66**, 12–21 (2010).
25. Petoukhov, M. V. et al. *J. Appl. Crystallogr.* **45**, 342–350 (2012).
26. Svergun, D., Barberato, C. & Koch, M. H. J. *J. Appl. Crystallogr.* **28**, 768–773 (1995).
27. Dominguez, C., Boelens, R. & Bonvin, A. M. J. J. *J. Am. Chem. Soc.* **125**, 1731–1737 (2003).
28. Holm, L. & Laakso, L. M. *Nucleic Acids Res.* **44**, W351–W355 (2016).
29. Sievers, F. et al. *Mol. Syst. Biol.* **7**, 539–539 (2011).
30. Chojnacki, S., Cowley, A., Lee, J., Foix, A. & Lopez, R. *Nucleic Acids Res.* **45**, W550–W553 (2017).
31. Ashkenazy, H. et al. *Nucleic Acids Res.* **44**, W344–W350 (2016).

nature research

Corresponding author(s): A Perrakis

Last updated by author(s): 5/13/2019

Reporting Summary

Nature Research wishes to improve the reproducibility of the work that we publish. This form provides structure for consistency and transparency in reporting. For further information on Nature Research policies, see Authors & Referees and the Editorial Policy Checklist.

Statistics

For all statistical analyses, confirm that the following items are present in the figure legend, table legend, main text, or Methods section.

n/a	Confirmed	
☐	☒	The exact sample size (*n*) for each experimental group/condition, given as a discrete number and unit of measurement
☐	☒	A statement on whether measurements were taken from distinct samples or whether the same sample was measured repeatedly
☒	☐	The statistical test(s) used AND whether they are one- or two-sided *Only common tests should be described solely by name; describe more complex techniques in the Methods section.*
☒	☐	A description of all covariates tested
☒	☐	A description of any assumptions or corrections, such as tests of normality and adjustment for multiple comparisons
☐	☒	A full description of the statistical parameters including central tendency (e.g. means) or other basic estimates (e.g. regression coefficient) AND variation (e.g. standard deviation) or associated estimates of uncertainty (e.g. confidence intervals)
☒	☐	For null hypothesis testing, the test statistic (e.g. *F*, *t*, *r*) with confidence intervals, effect sizes, degrees of freedom and *P* value noted *Give P values as exact values whenever suitable.*
☒	☐	For Bayesian analysis, information on the choice of priors and Markov chain Monte Carlo settings
☒	☐	For hierarchical and complex designs, identification of the appropriate level for tests and full reporting of outcomes
☒	☐	Estimates of effect sizes (e.g. Cohen's *d*, Pearson's *r*), indicating how they were calculated

Our web collection on statistics for biologists contains articles on many of the points above.

Software and code

Policy information about availability of computer code

Data collection	Descriptions of instruments are procedures for macromolecular structure and SAXS data acquisition are described in papers we cite in our methods.
Data analysis	All software for macromolecular structure determination and SAXS analysis are cited in the paper.

For manuscripts utilizing custom algorithms or software that are central to the research but not yet described in published literature, software must be made available to editors/reviewers. We strongly encourage code deposition in a community repository (e.g. GitHub). See the Nature Research guidelines for submitting code & software for further information.

Data

Policy information about availability of data

All manuscripts must include a data availability statement. This statement should provide the following information, where applicable:

- Accession codes, unique identifiers, or web links for publicly available datasets
- A list of figures that have associated raw data
- A description of any restrictions on data availability

The unique identifier for PDB deposition is stated in Table 1 (6NVQ) and a validation report is attached with this document.

Field-specific reporting

Please select the one below that is the best fit for your research. If you are not sure, read the appropriate sections before making your selection.

☒ Life sciences ☐ Behavioural & social sciences ☐ Ecological, evolutionary & environmental sciences

Life sciences study design

All studies must disclose on these points even when the disclosure is negative.

Sample size	Two biological replicates for Western blots used for quantification
Data exclusions	Diffraction data were excluded above a certain resolution according to standard crystallographic procedures are stated in table 1 and online methods.
Replication	Experiments for show Western blots have been repeated twice.
Randomization	n/a
Blinding	n/a

Reporting for specific materials, systems and methods

We require information from authors about some types of materials, experimental systems and methods used in many studies. Here, indicate whether each material, system or method listed is relevant to your study. If you are not sure if a list item applies to your research, read the appropriate section before selecting a response.

Materials & experimental systems

n/a	Involved in the study
☐	☒ Antibodies
☐	☒ Eukaryotic cell lines
☒	☐ Palaeontology
☒	☐ Animals and other organisms
☒	☐ Human research participants
☒	☐ Clinical data

Methods

n/a	Involved in the study
☒	☐ ChIP-seq
☒	☐ Flow cytometry
☒	☐ MRI-based neuroimaging

Antibodies

Antibodies used	eIF4G (Cell Signallinbg Technologies #2498), α-tubulin (DM1A; Santa Cruz #32293), Flag (CST, #2368), detyrosineted α-tubulin (Merck Millipore AB3201)
Validation	validation report available at manufacturers websites

Eukaryotic cell lines

Policy information about cell lines

Cell line source(s)	HeLa
Authentication	not authenticated
Mycoplasma contamination	negative in regular central tests
Commonly misidentified lines (See ICLAC register)	*Name any commonly misidentified cell lines used in the study and provide a rationale for their use.*